Science
AAAS

Observing the Average Trajectories of Single Photons in a Two-Slit Interferometer

Sacha Kocsis *et al.*

Science **332**, 1170 (2011);
DOI: 10.1126/science.1202218

Science (print ISSN 0036-8075; online ISSN 1095-9203) is published weekly, except the last week in December, by the American Association for the Advancement of Science, 1200 New York Avenue NW, Washington, DC 20005.

29. Y. Larionova, W. Stolz, C. O. Weiss, *Opt. Lett.* **33**, 321 (2008).
30. A. J. Daley, P. Zoller, B. Trauzettel, *Phys. Rev. Lett.* **100**, 110404 (2008).
31. N. G. Berloff, Turbulence in exciton-polariton condensates. Preprint available at http://arxiv.org/abs/1010.5225 (2010).

Acknowledgments: We thank S. Barbay, J. Bloch, R. Kuszelewicz, W. D. Phillips, L. P. Pitaevskii, and M. Wouters for useful discussions, and L. Martiradonna for the confocal masks. This work was supported by the IFRAF, CLERMONT4, and the Agence Nationale de la Recherche. A.B. and C.C. are members of the Institut Universitaire de France.

Supporting Online Material
www.sciencemag.org/cgi/content/full/332/6034/1167/DC1
Materials and Methods
Figs. S1 to S4

28 December 2010; accepted 11 April 2011
10.1126/science.1202307

Observing the Average Trajectories of Single Photons in a Two-Slit Interferometer

Sacha Kocsis,[1,2]* Boris Braverman,[1]* Sylvain Ravets,[3]* Martin J. Stevens,[4] Richard P. Mirin,[4] L. Krister Shalm,[1,5] Aephraim M. Steinberg[1]†

A consequence of the quantum mechanical uncertainty principle is that one may not discuss the path or "trajectory" that a quantum particle takes, because any measurement of position irrevocably disturbs the momentum, and vice versa. Using weak measurements, however, it is possible to operationally define a set of trajectories for an ensemble of quantum particles. We sent single photons emitted by a quantum dot through a double-slit interferometer and reconstructed these trajectories by performing a weak measurement of the photon momentum, postselected according to the result of a strong measurement of photon position in a series of planes. The results provide an observationally grounded description of the propagation of subensembles of quantum particles in a two-slit interferometer.

In classical physics, the dynamics of a particle's evolution are governed by its position and velocity; to simultaneously know the particle's position and velocity is to know its past, present, and future. However, the Heisenberg uncertainty principle in quantum mechanics forbids simultaneous knowledge of the precise position and velocity of a particle. This makes it impossible to determine the trajectory of a single quantum particle in the same way as one would that of a classical particle: Any information gained about the quantum particle's position irrevocably alters its momentum (and vice versa) in a way that is fundamentally uncertain. One consequence is that in Young's double-slit experiment one cannot determine through which slit a particle passes (position) and still observe interference effects on a distant detection screen (equivalent to measuring the momentum). Particle-like trajectories and wavelike interference are "complementary" aspects of the behavior of a quantum system, and an experiment designed to observe one neces-

[1]Centre for Quantum Information and Quantum Control and Institute for Optical Sciences, Department of Physics, University of Toronto, 60 St. George Street, ON M5S 1A7, Canada. [2]Centre for Quantum Dynamics, Griffith University, Brisbane 4111, Australia. [3]Laboratoire Charles Fabry, Institut d'Optique, CNRS, Université Paris-Sud, Campus Polytechnique, 2 avenue Augustin Fresnel, RD 128, 91127 Palaiseau cedex, France. [4]National Institute of Standards and Technology, 325 Broadway, Boulder, CO 80305, USA. [5]Institute for Quantum Computing, University of Waterloo, 200 University Avenue West, Waterloo, ON N2L 3G1, Canada.

*These authors contributed equally to this work.
†To whom correspondence should be addressed. E-mail: steinberg@physics.utoronto.ca

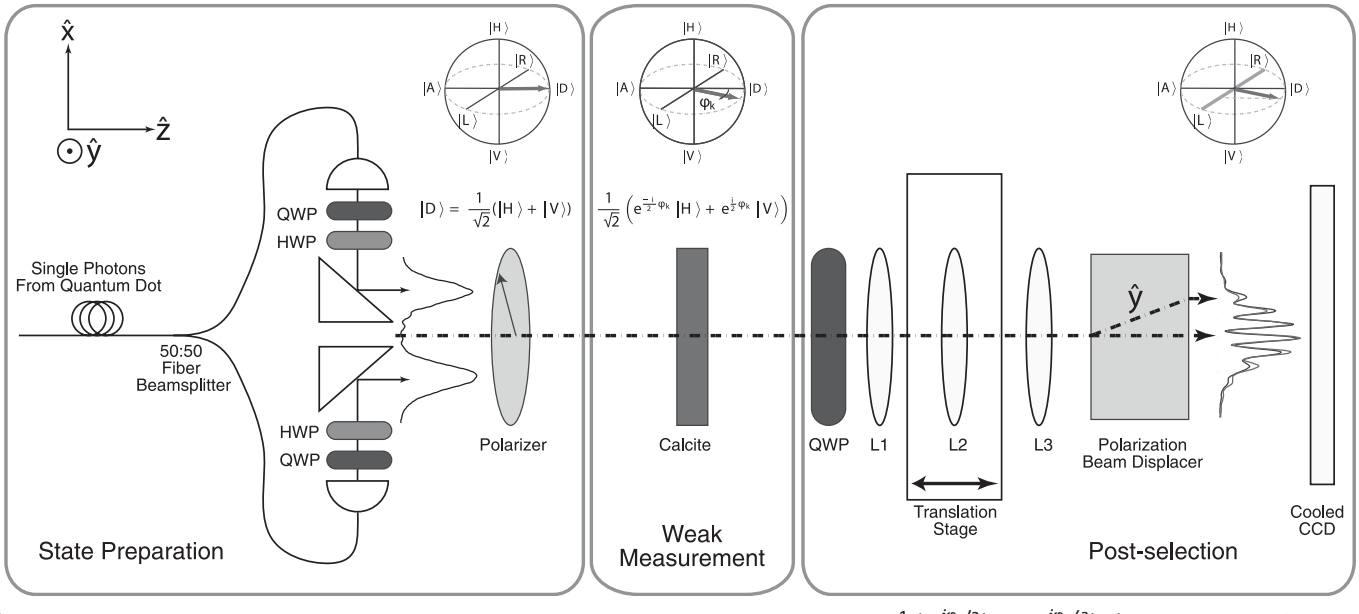

Fig. 1. Experimental setup for measuring the average photon trajectories. Single photons from an InGaAs quantum dot are split on a 50:50 beam splitter and then outcoupled from two collimated fiber couplers that act as double slits. A polarizer prepares the photons with a diagonal polarization $|D\rangle = \frac{1}{\sqrt{2}}(|H\rangle + |V\rangle)$. Quarter waveplates (QWP) and half waveplates (HWP) before the polarizer allow the number of photons passing through each slit to be varied. The weak measurement is performed by using a 0.7-mm-thick piece of calcite with its optic axis at 42° in the *x*-*z* plane that rotates the polarization state to $\frac{1}{\sqrt{2}}(e^{-i\varphi_k/2}|H\rangle + e^{i\varphi_k/2}|V\rangle)$. A QWP and a beam displacer are used to measure the polarization of the photons in the circular basis, allowing the weak momentum value k_x to be extracted. A cooled CCD measures the final *x* position of the photons. Lenses L1, L2, and L3 allow different imaging planes to be measured. The polarization states of the photons are represented on the Poincaré sphere, where the six compass points correspond to the polarization states $|H\rangle, |V\rangle, |D\rangle, |A\rangle = \frac{1}{\sqrt{2}}(|H\rangle - |V\rangle)$, $|L\rangle = \frac{1}{\sqrt{2}}(|H\rangle + i|V\rangle)$, and $|R\rangle = \frac{1}{\sqrt{2}}(|H\rangle - i|V\rangle)$.

sarily gives up the option of observing the other (*1*–*6*). However, it is possible to "weakly" measure a system, gaining some information about one property without appreciably disturbing the future evolution (*7*); although the information obtained from any individual measurement is limited, averaging over many trials determines an accurate mean value for the observable of interest, even for subensembles defined by some subsequent selection (perhaps even on a complementary observable). It was recently pointed out (*8*) that this provides a natural way to operationally define a set of particle trajectories: One can ascertain the mean momentum of the subensemble of particles that arrive at any given position, and, by thus determining the momentum at many positions in a series of planes, one can experimentally reconstruct a set of average trajectories. We use a modified version of this protocol to reconstruct the "weak-valued trajectories" followed by single photons as they undergo two-slit interference. In the case of single-particle quantum mechanics, the trajectories measured in this fashion reproduce those predicted in the Bohm–de Broglie interpretation of quantum mechanics (*9*, *10*).

Weak measurements, first proposed 2 decades ago (*7*, *11*), have recently attracted widespread attention as a powerful tool for investigating fundamental questions in quantum mechanics (*12*–*15*) and have generated excitement for their potential applications to enhancing precision measurement (*16*, *17*). In a typical von Neumann measurement, an observable of a system is coupled to a measurement apparatus or "pointer" via its momentum. This coupling leads to an average shift in the pointer position that is proportional to the expectation value of the system observable. In a "strong" measurement, this shift is large relative to the initial uncertainty in pointer position, so that significant information is acquired in a single shot. However, this implies that the pointer momentum must be very uncertain, and it is this uncertainty that creates the uncontrollable, irreversible disturbance associated with measurement. In a "weak" measurement, the pointer shift is small and little information can be gained on a single shot; but, on the other hand, there may be arbitrarily little disturbance imparted to the system. It is possible to subsequently postselect the system on a desired final state. Postselecting on a final state allows a particular subensemble to be studied, and the mean value obtained from repeating the weak measurement many times is known as the weak value. Unlike the results of strong measurements, weak values are not constrained to lie within the eigenvalue spectrum of the observable being measured (*7*). This has led to controversy over the meaning and role of weak values, but continuing research has made strides in clarifying their interpretation and demonstrating a variety of situations in which they are clearly useful (*16*–*21*).

In our experiment, we sent an ensemble of single photons through a two-slit interferometer and performed a weak measurement on each photon to gain a small amount of information about its momentum, followed by a strong measurement that postselects the subensemble of photons arriving at a particular position [see (*22*) for more details]. We used the polarization degree of freedom of the photons as a pointer that weakly couples to and measures the momentum of the photons. This weak momentum measurement does not appreciably disturb the system, and interference is still observed. The two measurements must be repeated on a large ensemble of particles in order to extract a useful amount of information about the system. From this set of measurements, we can determine the average momentum of the photons reaching any particular position in the image plane, and, by repeating this procedure in a series of planes, we can reconstruct trajectories over that range. In this sense, weak measurement finally allows us to speak about what happens to an ensemble of particles inside an interferometer.

Our quantum particles are single photons emitted by a liquid helium-cooled InGaAs quantum dot (*23*, *24*) embedded in a GaAs/AlAs micropillar cavity. The dot is optically pumped by a CW laser at 810 nm and emits single photons at

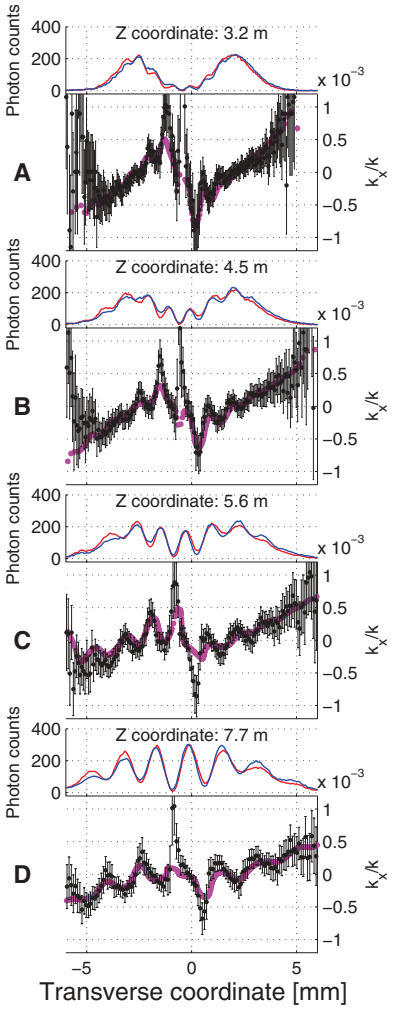

Fig. 2. Measured intensities (photon counts) of the two circular polarization components of $|\psi\rangle$, measured on the CCD screen (red and blue curves), as well as the weak momentum values calculated from these intensities (black) for imaging planes at (**A**) $z = 3.2$ m, (**B**) $z = 4.5$ m, (**C**) $z = 5.6$ m, and (**D**) $z = 7.7$ m. The red and blue data points are the intensity data with constant background subtracted. The errors for the momentum values were calculated by simulating the effect of Poissonian noise in the photon counts. The magenta curve shows momentum values obtained from enforcing probability density conservation between adjacent z planes. Because of the coarse-grained averaging over three imaging planes, the probability-conserving momentum values are not as sensitive as the measured weak momentum values to highly localized regions in the pattern with steep momentum gradients.

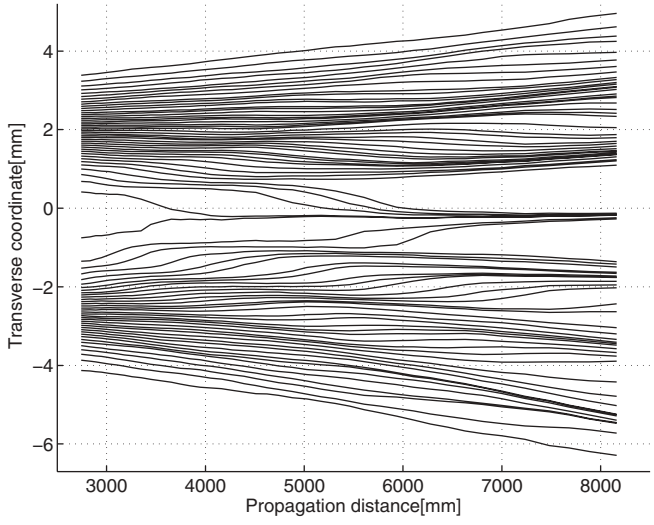

Fig. 3. The reconstructed average trajectories of an ensemble of single photons in the double-slit apparatus. The trajectories are reconstructed over the range 2.75 ± 0.05 to 8.2 ± 0.1 m by using the momentum data (black points in Fig. 2) from 41 imaging planes. Here, 80 trajectories are shown. To reconstruct a set of trajectories, we determined the weak momentum values for the transverse x positions at the initial plane. On the basis of this initial position and momentum information, the x position on the subsequent imaging plane that each trajectory lands is calculated, and the measured weak momentum value k_x at this point found. This process is repeated until the final imaging plane is reached and the trajectories are traced out. If a trajectory lands on a point that is not the center of a pixel, then a cubic spline interpolation between neighboring momentum values is used.

a wavelength λ of 943 nm. A Hanbury Brown-Twiss interferometer is used to measure a second-order correlation function $g^{(2)}(0)$ of 0.17 ± 0.04 (SD), confirming the single-photon nature of the dot emission (*25*). The photons are coupled into single-mode fiber and sent through an in-fiber 50:50 beam splitter. The outputs of the beam splitter exit two fiber launchers as Gaussian beams with their waists at the fiber launchers and are redirected to be parallel along the z axis by mirrored prisms to create the initial "slit function" (Fig. 1). The two Gaussian beams have a waist $1/e^2$ radius of 0.608 ± 0.006 mm and a peak-to-peak separation of 4.69 ± 0.02 mm. The polarization of the photons, which serves as the ancilla system for the weak measurement, is prepared in the initial state $|\psi\rangle = (1/\sqrt{2})(|H\rangle + |V\rangle)$, where $|H\rangle$ is identified with the x axis and $|V\rangle$ with the y axis.

The weak measurement is accomplished with a thin piece of birefringent calcite that changes the polarization of the photons passing through by introducing a phase shift between the ordinary and extraordinary components of polarization. The photons diffract out from the slits and impinge upon the crystal with an incident angle θ that depends on their transverse momentum k_x (where the momentum of a photon is $\mathbf{p} = \hbar\mathbf{k}$). By orienting the calcite's optic axis to lie in the x-z plane, $|H\rangle$ becomes the extraordinary polarization that encounters an angle-dependent index of refraction, $n_e(\theta)$, and $|V\rangle$ becomes the ordinary polarization that encounters a constant index of refraction, n_o. The calcite piece is 0.7 mm thick with its optic axis in the x-z plane at 42° to the z axis and imparts a small k_x-dependent birefringent phase shift that transforms the incident linear polarization state of the photons to a slightly elliptical polarization state. In this way, we carry out a measurement of the momentum with the polarization serving as a pointer that records the value of this observable. By arranging for the magnitude of the polarization rotation to be small with respect to the uncertainty in the photons' polarization, we ensure that the measurement is weak. No single measurement provides unambiguous information about the exact propagation direction, and hence no significant measurement disturbance is introduced. After averaging the results over many photons, it becomes possible to extract the average value of photon momentum.

The birefringent phase shift $\varphi(k_x)$ that the photons receive depends on the different paths and indices of refraction for the two polarizations in the calcite (*26*). The spread of the angles of the diffracting photons passing through calcite is small, allowing us to approximate the induced birefringent phase shift $\varphi(k_x)$ as a linear function of k_x:

$$\varphi(k_x) = \zeta \frac{k_x}{|\mathbf{k}|} + \varphi_0 \qquad (1)$$

The coefficient ζ designates the coupling strength between the phase we are measuring and the photon momentum, and its value was found to be 373.5 ± 3.4 (*22*). The calcite is tilted in the x-z plane to tune $\varphi_0 = 0$ modulo 2π.

A system of three cylindrical lenses, with the middle lens translatable in the z direction, allows the initial slit function to be imaged over an arbitrary distance. It is important to note that the thin calcite crystal performing the weak measurement remains fixed in place before the lenses. This does not affect the outcome of the final postselection at the various imaging planes along z as the interaction Hamiltonian between the polarization pointer and the photon's transverse momentum commutes with the free-progagation Hamiltonian of the system. The trajectories were reconstructed over the range 2.75 ± 0.05 to 8.2 ± 0.1 m to show the transition from the near-field to far-field intensity distribution. The polarization state of each photon is projected into the circular basis by using a quarter waveplate with its fast axis set to −45° to x, located in front of the lens system, and a polarizing beam displacer located behind the lenses. The beam displacer transmits the right-hand circularly polarized component of $|\psi\rangle$ undeviated and displaces the left-hand circularly polarized component of $|\psi\rangle$ vertically by about 2 mm. The photons are then detected on a cooled charge-coupled device (CCD). The exposure time on the CCD was set to 15 s, allowing the two vertically separated interference patterns to accumulate. During each exposure, about 31,000 single photons were detected by the CCD. By projecting into the circular basis, the momentum information encoded in polarization is transformed into an intensity modulation between the two vertically displaced patterns. The intensity of the top pattern (corresponding to the projection onto the right-hand circular polarization) is $I_R \propto [1 + \sin\varphi(k_x)]$, whereas the intensity of the bottom pattern (corresponding to the projection on to the left-hand circular polarization) goes as $I_L \propto [1 - \sin\varphi(k_x)]$. In the measured interference patterns at four different imaging planes (Fig. 2), the pixel on the CCD where each photon is detected corresponds to the photon's x position. The 26-μm pixel width sets the precision with which the photon's x position can be measured.

By using Eq. 1, we can simultaneously extract the weak value of the transverse component of the photon wave vector k_x at each pixel position

$$\frac{k_x}{|\mathbf{k}|} = \frac{1}{\zeta}\left[\sin^{-1}\left(\frac{I_R - I_L}{I_R + I_L}\right)\right] \qquad (2)$$

Thus for each value of the photon's position x, we are able to calculate the weak value of its transverse momentum k_x by taking the difference in modulated intensity between the two vertically displaced patterns at the same imaging plane along the z axis. The weak momentum values for four different imaging planes calculated in this way are shown in Fig. 2. By repeating the measurement for many imaging planes closely spaced along z, a vector field is produced from

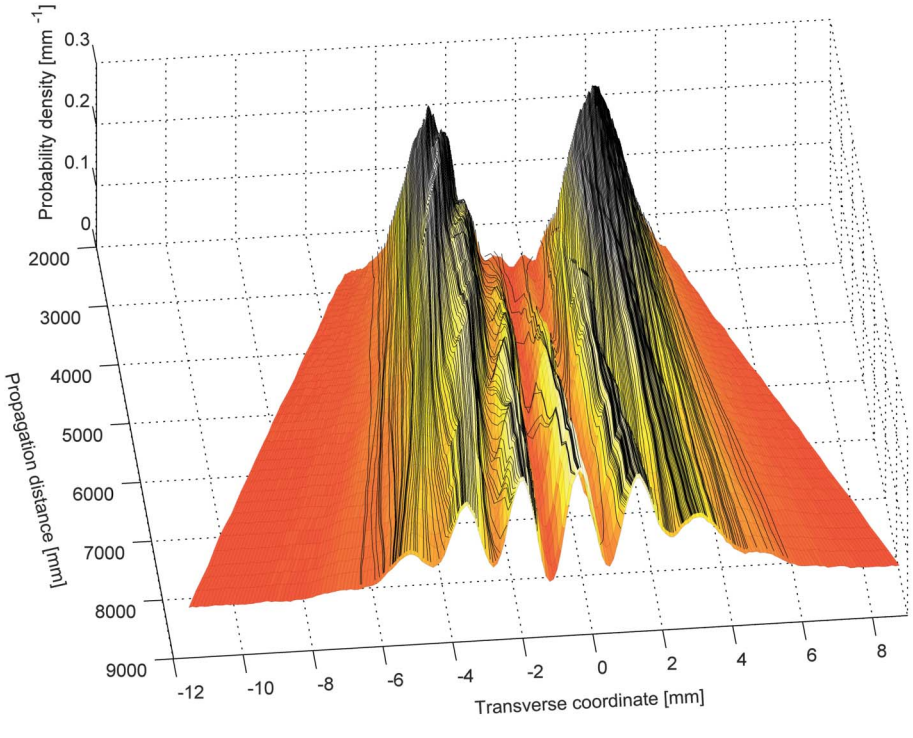

Fig. 4. The trajectories from Fig. 3 plotted on top of the measured probability density distribution. Even though the trajectories were reconstructed by using only local knowledge, they reproduce the global propagation behavior of the interference pattern.

which the weak-valued photon trajectories are reconstructed.

For the experimentally reconstructed trajectories for our double slit (Fig. 3), it is worth stressing that photons are not constrained to follow these precise trajectories; the exact trajectory of an individual quantum particle is not a well-defined concept. Rather, these trajectories represent the average behavior of the ensemble of photons when the weakly measured momentum in each plane is recorded contingent upon the final position at which a photon is observed. The trajectories resemble a hydrodynamic flow with a central line of symmetry clearly visible: Trajectories originating from one slit do not cross the central line of symmetry into the opposite side of the interference pattern. Trajectories at the edges of bright fringes tend to cross over to join more central bright fringes, thus generating the observed intensity distribution because of interference. The trajectories cross over dark fringes at relatively steep angles; there is a low probability of finding a photon in these regions that correspond to postselecting on a state nearly orthogonal to the initial state of the system. The separation of the imaging planes sets the scale over which features in the trajectories can be observed. The evolution of the interference in our double-slit apparatus takes place over a scale that is much longer than the separation between imaging planes, and our trajectories can accurately track the evolution of this interference. The one place where the accuracy can suffer is when a trajectory quickly passes through a dark fringe; here the fine scale behavior is smaller than the spacing between imaging planes. By overlaying the trajectories on top of the measured intensity distribution (Fig. 4), we observe that the trajectories reproduce the global interference pattern well. The tendency of the reconstructed trajectories to "bunch" together within each bright interference fringe is an artifact of measurement noise with the position error accumulating as the trajectory reconstruction is carried out further and further from the initial plane at $z = 2.75$ m. Single-particle trajectories measured in this fashion reproduce those predicted by the Bohm–de Broglie interpretation of quantum mechanics (*8*), although the reconstruction is in no way dependent on a choice of interpretation.

Controversy surrounding the role of measurement in quantum mechanics is as old as the quantum theory itself, and nowhere have the paradoxes been thrown into such stark relief as in the context of the double-slit experiment. Our experimentally observed trajectories provide an intuitive picture of the way in which a single particle interferes with itself. It is of course impossible to rigorously discuss the trajectory of an individual particle, but in a well-defined operational sense we gain information about the average momentum of the particle at each position within the interferometer, leading to a set of "average trajectories." The exact interpretation of these observed trajectories will require continued investigation, but these weak-measurement results can be grounded in experimental measurements that promise to elucidate a broad range of quantum phenomena (*7*, *11*–*13*, *15*–*17*). By using the power of weak measurements, we are able to provide a new perspective on the double-slit experiment, which Feynman famously considered to have in it "the heart of quantum mechanics" (*27*).

References and Notes

1. N. Bohr, *Collected Works* (North-Holland, Amsterdam, 1972).
2. W. K. Wootters, W. H. Zurek, *Phys. Rev. D* **19**, 473 (1979).
3. N. Bohr, *Naturwissenschaften* **16**, 245 (1928).
4. M. O. Scully, B.-G. Englert, H. Walther, *Nature* **351**, 111 (1991).
5. C. Brukner, A. Zeilinger, *Phys. Rev. Lett.* **83**, 3354 (1999).
6. V. Jacques *et al.*, *Science* **315**, 966 (2007).
7. Y. Aharonov, D. Z. Albert, L. Vaidman, *Phys. Rev. Lett.* **60**, 1351 (1988).
8. H. Wiseman, *N. J. Phys.* **9**, 165 (2007).
9. D. Bohm, *Phys. Rev.* **85**, 166 (1952).
10. D. Bohm, *Phys. Rev.* **85**, 180 (1952).
11. N. W. M. Ritchie, J. G. Story, R. G. Hulet, *Phys. Rev. Lett.* **66**, 1107 (1991).
12. R. Mir *et al.*, *N. J. Phys.* **9**, 287 (2007).
13. J. S. Lundeen, A. M. Steinberg, *Phys. Rev. Lett.* **102**, 020404 (2009).
14. K. Yokota, T. Yamamoto, M. Koashi, N. Imoto, *N. J. Phys.* **11**, 033011 (2009).
15. G. J. Pryde, J. L. O'Brien, A. G. White, T. C. Ralph, H. M. Wiseman, *Phys. Rev. Lett.* **94**, 220405 (2005).
16. O. Hosten, P. Kwiat, *Science* **319**, 787 (2008); 10.1126/science.1152697.
17. P. B. Dixon, D. J. Starling, A. N. Jordan, J. C. Howell, *Phys. Rev. Lett.* **102**, 173601 (2009).
18. A. Peres, *Phys. Rev. Lett.* **62**, 2326 (1989).
19. A. J. Leggett, *Phys. Rev. Lett.* **62**, 2325 (1989).
20. Y. Aharonov, L. Vaidman, *Phys. Rev. Lett.* **62**, 2327 (1989).
21. J. Dressel, S. Agarwal, A. N. Jordan, *Phys. Rev. Lett.* **104**, 240401 (2010).
22. Materials and methods are available as supporting material on *Science* Online.
23. R. P. Mirin, *Appl. Phys. Lett.* **84**, 1260 (2004).
24. R. H. Hadfield *et al.*, *Opt. Express* **13**, 10846 (2005).
25. R. Loudon, *The Quantum Theory of Light* (Oxford Univ. Press, Oxford, ed. 3, 2000).
26. M. Born, E. Wolf, *Principles of Optics* (Cambridge Univ. Press, Cambridge, 1999).
27. R. Feynman, *The Feynman Lectures on Physics* (Addison-Wesley, Boston, 1989).

Acknowledgments: A.M.S. conceived of the experiment and supervised the work; M.J.S. and R.P.M. designed and fabricated the single-photon sources; S.K. constructed the experiment and acquired the data with assistance from B.B. and S.R. and much guidance from L.K.S.; B.B., S.K., and S.R. carried out the data analysis and generated the figures; S.K. and L.K.S. wrote the text with input from all the other co-authors. This work was supported by the Natural Sciences and Engineering Research Council of Canada, the Canadian Institute for Advanced Research, and QuantumWorks. S.K. thanks B. Higgins and L.K.S. thanks K. J. Resch for useful discussions. The data from the experiment has been archived and is available at www.physics.utoronto.ca/~aephraim/data/PhotonTrajectories.

Supporting Online Material

www.sciencemag.org/cgi/content/full/332/6034/1170/DC1
Materials and Methods

27 December 2010; accepted 11 April 2011
10.1126/science.1202218

Spin-Liquid Ground State of the $S = 1/2$ Kagome Heisenberg Antiferromagnet

Simeng Yan,[1] David A. Huse,[2,3] Steven R. White[1]*

We use the density matrix renormalization group to perform accurate calculations of the ground state of the nearest-neighbor quantum spin $S = 1/2$ Heisenberg antiferromagnet on the kagome lattice. We study this model on numerous long cylinders with circumferences up to 12 lattice spacings. Through a combination of very-low-energy and small finite-size effects, our results provide strong evidence that, for the infinite two-dimensional system, the ground state of this model is a fully gapped spin liquid.

We consider the quantum spin $S = 1/2$ kagome Heisenberg antiferromagnet (KHA) with only nearest-neighbor isotropic exchange interactions (Hamiltonian $H = \Sigma \vec{S}_i \cdot \vec{S}_j$, where $\vec{S}_i$ and $\vec{S}_j$ are the spin operators for sites i and j, respectively) on a kagome lattice (Fig. 1A). This frustrated spin system has long been thought to be an ideal candidate for a simple, physically realistic model that shows a spin-liquid ground state (*1*–*3*). A spin liquid is a magnetic system that has "melted" in its ground state because of quantum fluctuations, so it has no spontaneously broken symmetries (*4*). A key problem in searching for spin liquids in two-dimensional (2D) models is that there are no exact or nearly exact analytical or computational methods to solve infinite 2D quantum lattice systems. For 1D systems, the density matrix renormalization group (DMRG) (*5*, *6*), the method we use here, serves in this capacity. In addition to its interest as an important topic in quantum magnetism, the search for spin liquids thus serves as a test-bed for the development of accurate and widely applicable computational methods for 2D many-body quantum systems.

[1]Department of Physics and Astronomy, University of California, Irvine, CA 92617, USA. [2]Department of Physics, Princeton University, Princeton, NJ 08544, USA. [3]Institute for Advanced Study, Princeton, NJ 08540, USA.

*To whom correspondence should be addressed. E-mail: srwhite@uci.edu